THE JOURNAL OF BIOLOGICAL CHEMISTRY
Vol. 268, No. 24, Issue of August 25, pp. 17908-17916, 1993
Printed in U.S.A.

Molecular Dynamics Simulation of No Recombination to Myoglobin Mutants*

(Received for publication, February 19, 1993, and in revised form, April 20, 1993)

Haiying Li and Ron Elber‡§

From the Department of Chemistry, University of Illinois, Chicago, Illinois 60680 and the ‡Department of Physical Chemistry, Fritz Haber Research Center and Institute of Life Sciences, The Hebrew University, Givat Ram, Jerusalem 91904, Israel

John E. Straub

From the Department of Chemistry, Boston University, Boston, Massachusetts 02215

Molecular dynamics simulations on two coupled electronic surfaces are employed to investigate the geminate recombination of nitric oxide to mutants of sperm whale myoglobin. A model for the ground and the excited states is constructed based on experimental data. The crossing between the surfaces is treated using the Landau-Zener formula. The reaction probability and the recombination curves are calculated directly by histogramming the results of an ensemble of trajectories. The experimental trend is reproduced in which the picosecond recombination rate of different mutants increases in the order $Phe^{29} > Leu^{29} > Val^{29} > Ala^{29}$. Furthermore, in accord with the experiment on significantly longer time scales an opposite trend is obtained, in which the recombination rate for Ala^{29} is larger than for Phe^{29}. These results are explained by constrained diffusion of the ligand in the heme pocket. The average and the transient volume of the heme pocket is modified by the 29 mutants.

Computer simulations of the interactions of small ligands with heme proteins have advanced considerably during the last few years. This is due to the rapid growth in computer technology and to the parallel developments in new simulation techniques (1-4). Equally important are the significant enhancements of experimental methodologies that provided stimulating and detailed data. Most relevant to the present article is the introduction of short laser pulses and the availability of myoglobin mutants (5-9). The mutants make it possible to study the influence of individual residues on the recombination process.

The experimental set up of interest to us is that of geminate recombination. There, a short laser pulse is used to dissociate the ligand that is bound to the heme (here we consider only the diatomic ligand, nitric oxide), and the rate of ligand recombination to the heme is measured. The rate of recombination provides information (in an indirect way) on the ligand diffusion in the protein matrix and on the interactions of the ligand with the protein residues (10). Understanding of the geminate recombination process was advanced significantly by simulation of the ligand diffusion (1-4) and in one case by constructing a simplified model of the recombination (11). However, in order to fully appreciate what the geminate recombination can teach us about the motion of the ligand it is important to carry out simulations which can be related *directly* to raw experimental data; that is, to compute directly the recombination curves. This is the goal of the present paper in which a complete computational model for the geminate recombination process is presented.

Effort was made to evaluate the quality of the model directly against the recombination experiments without any further simplifications or approximations beyond the classical trajectory simulation techniques. For example, the equilibrium assumption of the transition state theory (2, 4) may be questionable for the process under investigation (10), and it is therefore avoided. Even approximations that were shown in the past to give useful results (such as the Locally Enhanced Sampling methodology (1, 11)) are not quantitative. Therefore, the rebinding curves were calculated in the most straightforward way that we could afford computationally. An ensemble of trajectories is initiated on the electronically excited state. The trajectories are propagated numerically in small time steps, and the number of trajectories that do not rebind is calculated as a function of time. These trajectories reflect the concentration of the dissociated heme that is measured experimentally. Since the calculations are pursued in a direct way, they can also serve as a future reference and as a test of approximate theories that may require considerably less computer resources.

In the following sections, we describe the parameters of the model together with the Landau-Zener scheme used to describe the jumps between the electronic surfaces and we outline the computational protocol.

EXPERIMENTAL PROCEDURES

Computational Model and Protocol—All the calculations presented in this paper were performed using the program MOIL.[1] The potential energy function of MOIL is the combination of AMBER/OPLS (13, 14) with improper torsions adopted from the CHARMM force field (15). The parameters of Kuczera *et al.* (16) (see Table I) for the heme force field were used, unless specifically stated otherwise in the text. Kuczera *et al.* provided the parameters for the six coordinated and five coordinated heme iron.

In constructing the ground and the excited state potentials between the nitric oxide and the heme we used (as much as possible) pieces of independent experimental data. Ab-inito calculations (17) can provide qualitative understanding of the coupling and of the ordering of

* This research was supported in part by National Institutes of Health Grant GM41905 (to R. E.) and by the Minnerva Fund. The costs of publication of this article were defrayed in part by the payment of page charges. This article must therefore be hereby marked "*advertisement*" in accordance with 18 U.S.C. Section 1734 solely to indicate this fact.

§ University of Illinois West Scholar and Alon fellow in the Hebrew University.

[1] Elber, R., Roitberg, A., Verkhivker, G., Goldstein, R., Li, H., and Simmerling, C. (1993) *Statistical Mechanics and Protein-Substrate Interactions*, NATO Workshop, Corsica, in press.

TABLE I

Heme Parameters

Atom Names: Np, heme pyrrole nitrogen; CPA CPB CPM, heme α, β, and *meso* carbons; HA, hydrogen bound to CPM; CH2E CH3E, extended carbon atoms with two or three hydrogens, in heme substituents; CR1E, extended atom for aromatic carbon with one hydrogen in heme vinyl substituents; NB, the proximal histidine nitrogen (NE2) to which the iron is attached; CP and CF are the CE1 and CD2 atoms of the proximal histidine; CO, OC, carboxyl carbon and carboxyl oxygen, respectively; NM, OM, nitric oxide nitrogen and oxygen atoms; FE, FE1, iron atoms for heme with six ligands and for heme with five ligands, respectively. When parameters of FE1 are not provided explicitly the same parameters as for FE should be used. Units: Force constants (k) are given by kcal/mol Å^{-2} for bonds kcal/mol radians^{-2} for angles, kcal/mol for torsions, and kcal/mol radians^{-2} for improper torsions. Bond distances are given in angstroms and values for angles in degrees. The periodicity parameter for torsions (n) has (of course) no units. The non-bonded parameters include charge (units of the electron charge), ϵ the van der Waals well depth (kcal/mol), and σ (Å). The combination rules for the non-bonded parameters are those of the OPLS force field (14) as implemented in MOIL.[1]

Bonds

Pair	k	r
FE-Np	270.2	1.9569
FE1-Np	270.2	2.1000
Np-CPA	377.2	1.3757
CPB-CPB	340.7	1.3464
CPM-HA	367.6	1.0900
CPB-CH3E	441.3	1.5200
CH2E(2)-CO	405.0	1.5200
CH2E(2)-CR1E	250.0	1.4500
CPA-CPB	299.8	1.4432
CPA-CPM	360.0	1.3716
CPB-CH2E(1)	441.3	1.5200
CPB-CR1E	441.3	1.3800
CO-OC	656.0	1.2500
CH2E(1)-CH2E(2)	225.0	1.5200
FE-NM	109.6	1.743
FE-NB	65.0	2.2
FE1-NB	65.0	2.1
NM-OM	826.9	1.150

Angles

Pair	k	Θ
FE-NM-OM	35.0	153.0
FE-NB-CF	30.0	120.0
NB-FE-NM	50.0	180.0
FE-NB-CP	30.0	130.0
NB-FE-NP	50.0	90.0
NB-FE1-NP	50.0	107.0
NP-FE-NP	50.0	90.0
NP-FE1-NP	80.0	90.0
CPA-NP-CPA	139.3	103.90
NP-CPA-CPM	88.0	124.39
CPA-CPM-HA	12.70	117.44
CPB-CPA-CPM	61.60	124.07
CPA-CPM-CPA	94.02	125.12
CPB-CPB-CH3E	65.00	126.75
CPB-CPB-CH2E(1)	65.00	126.75
CPB-CPB-CR1E	70.00	126.75
CPB-CH2E(1)-CH2E(2)	70.00	113.00
CH2E(1)-CH2E(2)-CO	70.00	113.00
OC-CO-OC	85.00	120.00
CH2E(2)-CO-OC	85.0	121.60
CPA-CPB-CH2E(1)	65.0	126.75
CPA-CPB-CR1E	70.0	126.75
CPB-CR1E-CH2E	70.0	121.50

Angles

Pair	k	Θ
CPA-NP-FE	96.15	128.05
NP-CPA-CPB	122.00	111.54
CPA-CPB-CH3E	65.00	126.75

Torsions

	K	n	Φ
X-FE-NM-X	0.0	3	0.0
X-FE-NB-X	0.0	3	0.0
X-CH2E(2)-CH2E(1)-X	1.6	3	0.0
X-CPA-CPB-X	10.15	2	180.0
X-CPB-CR1E-X	10.4	2	180.0
X-CPA-NP-X	5.2	2	180.0
X-CPA-CPM-X	4.58	2	180.0

Improper torsions

	K	Φ
CPB-CPA-CPB-CR1E	90.0	0.0
CPA-CPB-CPM-NP	32.70	0.0
CPB-CPA-CPB-CH2E(1)	90.0	0.0
NP-FE-CPA-CPA	137.4	0.0
CPB-CPA-CPB-CH3E	90.0	0.0
CO-CH2E(2)-OC-OC	100.0	0.0
CPM-CPA-HA-CPA	29.40	0.0

Nonbonded

	Charge	ϵ	σ^a
FE	0.24	0.0	1.16
CPA	0.03	0.12	3.74
HA	0.00	0.045	2.62
CPB2	0.02	0.12	3.74[a]
CH2E(1)	0.04	0.114	3.98
CH3E	−0.04	0.18	3.86
CR1E	0.03	0.12	3.74
NP	−0.18	0.2384	2.85
CPM	0.04	0.12	3.74
CPB1	−0.02	0.12	3.74[a]
CPB3	−0.05	0.12	3.74[a]
CH2E(2)	−0.10	0.1140	3.98
CO	0.30	0.105	3.75
OC	−0.5	0.21	2.96
NM	0.028	0.17	3.25
OM	−0.028	0.159	3.12

[a] Covalent = CPB.

orbitals but not potential energy surfaces of the quality needed for semiquantitative studies of recombination.

We consider two curves describing the interaction of the NO with the heme iron, a ground state and a single excited state. In the ground state there is a strong bond between the ligand and the heme (from thermodynamic data (18) the binding energy is estimated to be 30 kcal/mol; the effect of zero point energy is negligible). The ground state is modeled by a Morse curve,

$$V_g(R_{N\text{-}Fe}) = D(e^{-2\alpha x} - 2e^{-\alpha x}) \qquad \text{(Eq. 1)}$$

where D is the binding energy (D = 30 kcal/mol), α is the range parameter (α = 2 Å^{-1}) and x is the deviation of the nitrogen-iron distance ($R_{N\text{-}Fe}$) from the equilibrium value (R_o). The range parameter was estimated from the known vibrational frequency of the nitrogen-iron bond (19). For the Morse potential the vibrational frequency is given by $\omega = [2\alpha^2 D/M]^{1/2}$ where M is the reduced mass of the nitrogen-iron bond.

To the potential describing the bonded system, we also added an angle term describing the relative orientation of the Fe-N bond with respect to the N-O bond. The orientation of nitric oxide is known from experiments; the NO axis is bent by 27 degrees with respect to the normal to the heme plane. The usual energy term for angles is added $(1/2)K(\Theta - \Theta_{eq})^2$ where K is the force constant (K = 70 kcal/mol radians^{-2}), Θ is the angle between the two bonds (Fe-N and N-

O) and Θ_{eq} is the equilibrium position ($\Theta_{eq} = 153°$). The van der Waals parameters of NO are: $\epsilon(N) = 0.17$ kcal/mol, $\sigma(N) = 3.25$ Å, $\epsilon(O) = 0.159$ kcal/mol, $\sigma = 3.12$ Å. The combination rules are those given for the optimized potential for liquid simulations force field (14).

The parameters of the excited state are less reliable. It is not even obvious if a *single* excited state is sufficient to describe the photodissociation process. Nevertheless, we use a model of a single excited state which is the simplest that we can use and still account (at least qualitatively) for the available experimental data.

For the excited state we use a similar functional form to that employed by Agmon and Hopfield (20) in their diffusion model of carbon monoxide recombination. Our potential parameters are, however, very different. We also use a theoretical approach different from the one used by Agmon and Hopfield. The process which they modeled takes longer times than the process on which our attention is focused. For the geminate recombination of carbon monoxide, the diffusion equation is likely to be appropriate. For the short time scales on which the nitric oxide rebinds to the heme iron, more detailed modeling is required.

A single exponential function is used to model the excited state,

$$V_e(R_{N-Fe}) = A \exp(-bR_{N-Fe}) - B \qquad \text{(Eq. 2)}$$

The excited state is shifted by B ($B = 4$ kcal/mol) with respect to the asymptotic (dissociated) energy of the ground state. b is a range parameter for the repulsive curve ($b = 1$ Å^{-1}) and $A = 80$ kcal/mol. A and b are interdependent. We assume a vertical transition from the instantaneous position sampled during a trajectory on the ground state to the excited state. The assigned value for b determines an upper bound for A, based on the photon energy. In Fig. 1 we show the two one-dimensional curves of nitric oxide-heme iron interaction used in our model. The plot does not show three other changes that happen in the simulated system in the event of photodissociation: 1) the angle term for the Fe-N-O is removed, 2) the exclusion list for non-bonded interactions is updated, and 3) the heme potential is switched to the unbound form (see below). Before the dissociation the van der Waals interaction of the ligand with the iron and pyrrole nitrogens was set to zero. Once the system reaches the excited state, these interactions are turned on.

For a recombination to occur, it is necessary for the ligand to switch from the excited state back to the ground state. Such a switch is most likely to take place when the two electronic states are degenerate, *i.e.* in the domain of curve crossing in which the Born-Oppenheimer approximation is not valid. Transitions between electronic curves that cross at one point can be described by a semiclassical formula developed by Landau and Zener (21, 22). The Landau-Zener theory was combined in the past with classical trajectory calculations to measure the *equilibrium* activated rate constant on a model system (23, 24). Here ordinary classical trajectories are used everywhere except near the crossing point at which a classical trajectory has a significant probability of switching to the other potential curve. The probability P of the system to remain on the adiabatic surface in a single pass of the crossing point is

$$P = 1 - \exp(-\pi\ \Gamma_{LZ}/2) \qquad \text{(Eq. 3)}$$

where Γ_{LZ} is given by

$$\Gamma_{LZ} = (2\pi\Delta^2)/(h\upsilon\,|\,F_1 - F_2\,|) \qquad \text{(Eq. 4)}$$

F_1 and F_2 are the slopes of the diabatic curves at the crossing point, h is the Planck constant, υ is the classical velocity along the reaction coordinate (the distance between the nitrogen and the iron in our model) and Δ is the electronic coupling between the two curves. The "decision" as to on which of the curves the ligand will continue moving on is made as follows: when the ligand enters the crossing zone (which is defined as $\Delta/|F_1\text{-}F_2|$ in the neighborhood of the curve crossing point) the probability P is calculated using the coordinates and the velocities at this particular time. P is then compared to a random number, r, sampled from a uniform distribution between 0 and 1. If r is less than or equal to P the system stays on the adiabatic energy surface, otherwise a switch occurs.

The underlying assumption of this protocol (which is also the main assumption in the derivation of the Landau-Zener formula) is that the resident time of the system in the crossing zone is very short. This makes it possible to approximate the trajectory of the particle as ballistic (21, 22) and also to calculate P only once per crossing, at the time at which the ligand enters the crossing zone.

After an appropriate ensemble of trajectories is generated for some specific Δ value, it is possible to recalculate from this single set of trajectories the corresponding set of trajectories for different Δ-s (or P-s). Consider the original set of trajectories that employed a specific Δ value, say Δ_1, that gave a set of transition probabilities P_1. In the new set Δ_2 should be employed, and this leads to a new set of transition probabilities P_2. To obtain the appropriate branching ratio between the curves, we change the relative weight of the trajectories when averages are calculated. In the original set of N trajectories, each trajectory was weighted by 1/N. In the new set a trajectory that passes J times through the crossing point will have a weight (W) of

$$W = \prod_{j=1}^{J} P_{2j}/P_{1j} \qquad \text{(Eq. 5)}$$

The recombination probability will now be the sum of the weights of trajectories that recombine divided by the weight of all trajectories.

To have a reasonable value of Δ to start with, we adopted an estimated value for O_2. The electronic spin changes in the rebinding of NO and O_2 are the same (one spin unit). We therefore assume that Δ is similar for both ligands and can be estimated as $\Delta = 200$ cm^{-1} (25). Different ensembles of trajectories can be constructed based on the formula written above.

Another experimental observation is the relaxation of the heme from the bonded configuration in which the iron is in the heme plane to the unbonded configuration in which the iron is displaced out of the heme by approximately 0.4 Å. We require that our model will give the correct results in the two asymptotic limits of fully unbonded (U_u) and fully bonded (U_b) force fields. The asymptotic potentials are taken from Ref. 16. For the completeness of the paper, we provide in the "Appendix" a complete list of all the heme parameters. There are two options for the use of the heme potential. If the ligand is moving on the excited repulsive state, only U_u is employed. If the ligand is moving on the binding curve, then, the potential is switched from U_u at large ligand iron distances to U_b at short ligand iron distances. A switching function between the two heme potentials is defined for nuclear motion on the electronic ground state potential surface, as follows:

$$U_h = fU_u + (1 - f)U_b \qquad \text{(Eq. 6)}$$

where f is a switching function.

$$f = 1/[1 + \exp(-\lambda(R_{N-Fe} - R_{cut}))] \qquad \text{(Eq. 7)}$$

The switching function changes from zero to one depending on the distance $R_{N\text{-}Fe}$. We varied R_{cut} and λ parameters in the range $R_{cut} =$ 3,4 and $\lambda = 3$–5 and calculated the recombination curves for the four mutants. In the calculations presented in this paper, R_{cut} is set to 3 Å and λ to 5 Å^{-1}. R_{cut} is placed close to the crossing point and is correlated with the value of B. Changing R_{cut} to 4 Å has a negligible

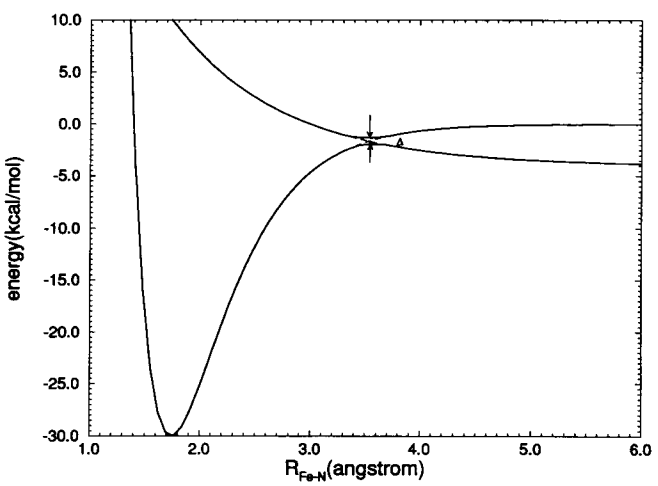

FIG. 1. **The ground and the excited electronic energy surfaces for the interaction between the nitrogen in nitric oxide and the heme iron.** The plot includes only the Morse curve (the ground state) and the exponential repulsion (excited state). It is shown for an optimal orientation of the NO with respect to the heme plane. The barrier for a ligand approaching the bound state on the lower curve is 2.3 kcal/mol.

effect on the results of the recombination. The results were also insensitive to the value of λ.

This completes the description of the geminate recombination model. We summarize below the main additions to the molecular dynamics program MOIL[1] to make it possible to simulate geminate recombination.

(*a*) Two crossing potential energy surfaces are introduced.

(*b*) Classical trajectories are calculated on these surfaces, and crossing between the ground and the excited states is modeled via the Landau-Zener formula.

(*c*) To describe mechanical dissociation of the ligand (*i.e.* stretching the ligand-iron bond until it breaks without changing the electronic energy surface), a switching function for the heme is introduced. This is since at short distances the iron tends to be in the heme plane while forming a bond with the ligand, and at larger distances the iron is displaced out of the heme plane. The heme parameters are therefore modified.

Computational Protocol—The simulation of geminate recombination in the picosecond time regime is pursued by averaging over trajectories that mimic the photodissociation process. The recombination time is simply too short to justify the use of equilibrium ideas such as the one employed in the transition state theory. Thus, it is very unlikely that the dissociated system approaches equilibrium on this time scale. It is more likely that the recombination occurs from a collection of structures that are only partially equilibrated. Strong evidence for the "nonequilibrium" characteristics of the process is provided by the experiments initiated by Austin *et al.* (10). These experiments demonstrate that in parallel to the recombination process considerable relaxation takes place within the protein. The simulations were therefore pursued as follows. For each of the mutants, the bound state (with NO) was minimized for 300 conjugate gradient steps, starting from the x-ray coordinates of the mutants (8). We investigated the wild type (Leu^{29}), Phe^{29}, and Val^{29} mutants. The initial conformation for the Ala^{29} mutant (for which a crystal structure is not available) was modeled by using the β carbon of Leu^{29} for the position of the alanine residue in the corresponding mutant. The rest of the coordinates were left untouched.

It should be noted that according to the x-ray data (8) the 29 mutants have highly conserved structures. Thus, the structural modifications are limited to the mutated residues and are not extended over a significant portion of the protein molecule. The minimized coordinates were heated linearly in time to 300 K over the period of 10 ps and were equilibrated for an additional 10 ps. Structures were sampled at random from the 10 ps equilibrium run of the bonded trajectories and were used to initiate 100 trajectories of the photodissociated ligands. Ten structures were sampled at intervals of 0.1 ps. Each of these structures was used to initiate 10 trajectories by selecting different initial velocities. The trajectories with different velocities diverge very quickly. Each of the trajectories was initiated with random velocities sampled from the Boltzmann distribution, while the potential energy used to initiate the simulation of the photodissociation process was that of the *excited state*. Hence, the transition induced by the light is assumed vertical without a change in the coordinates or the velocities of the atoms. The trajectory is then propagated using the standard classical equations of motion on the excited state potential until it approaches the crossing point. The fate of the trajectory (to cross or not to cross?) is then decided according to the prescription described under the Computational Model section.

The interest is focused on four different mutants at the 29-position of a cloned sperm whale myoglobin (8, 11). In Fig. 2 we show the relevant residues at the active site for the wild type. The unique feature of these mutations is that they do not interact directly with the heme. Therefore, one can reasonably assume that they probe *the ligand dynamics* and not (for example) changes in the interactions of the protein with the heme. The 100 trajectories for each of the mutants were terminated after a 10-ps production run. At each tenth of a picosecond the results were analyzed. If the value of the Morse potential energy that describes the interaction of the nitrogen with the iron was negative and at least −10 kcal/mol, the ligand was considered bonded. A dissociated ligand-iron bond was assumed when the interaction potential was close to zero (less than −0.1 kcal/mol). No "intermediate cases" were found. For these short time scales, we did not expect the solvent to play a major role, and therefore explicit treatment of the solvent was not added to the protein simulations. A few trajectories were rerun with a solvation shell. The size of the shell varied from several tens (the crystallographic water) to a complete solvation shell of 5 Å thickness (800 water molecules). The results of the more elaborate calculations were very similar to those without the solvent for the model of the ligand employed in this work. Therefore the cheaper approach without solvent was used throughout the remainder of the study.

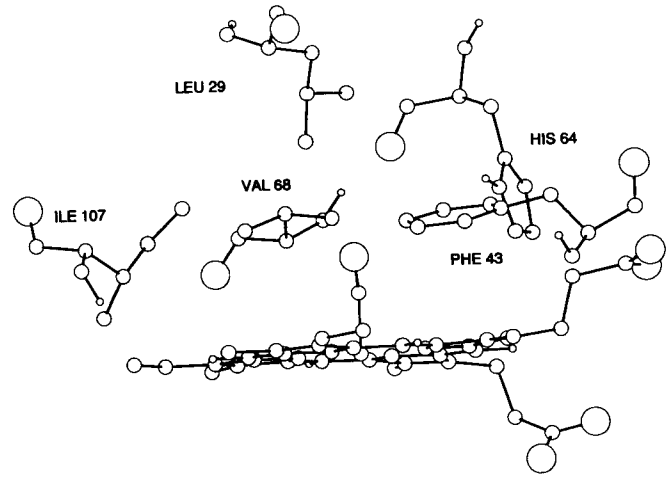

FIG. 2. **A stick and ball model of the heme pocket, the bound ligand, and several important residues that include Leu^{29}, Phe^{43}, His^{64}, Val*68*, and Ile^{107}.**

Finally, 36 trajectories of 500 ps each were used to examine the long time recombination kinetics in both Phe^{29} and Ala^{29}. This was done by picking trajectories that did not rebind after 10 ps and continuing the simulations for additional 500 ps.

RESULTS

In Fig. 3*a* we show recombination curves calculated using the model described above. In spite of the short time scale (due to which it is difficult to compare the results quantitatively to the experimental data) a few points are worth stressing. First the order of the recombination yields, $Phe^{29} > Leu^{29}$ (native) $> Val^{29} > Ala^{29}$, agrees with the experimental data. It should be noted that this result is not easy to obtain; *e.g.* in an earlier investigation employing the approximate methodology LES (11), the valine and the leucine results were very similar. In fact, considerable work and trial and error were required to determine the excited state and the crossing parameters so that the correct trend will be reproduced. The comparative study of the recombination in a series of mutants provides a strict test of the quality of the computational model. We also comment that the extracted recombination curves for $\Delta = 100\ cm^{-1}$ are in reasonable qualitative agreement with fast recombination data (26) that were collected for the wild type only. In a 10-ps period, 82% of the population survived in the experiment and 72% survived in the simulation. At this point the model satisfies the objectives we set to ourselves at the beginning of the study of reproducing the qualitative results on the short time dynamics and other experimental data. Now we should like to extract from the simulation more information on the protein and the ligand dynamics.

One question of interest is what are the protein coordinates that relax in parallel with the ligand dissociation and how this relaxation affects the geminate recombination. In Fig. 4*a* we show the relaxation of the heme iron from the in-plane position to the out-of-plane position. The results of four trajectories of the Phe^{29} mutant are shown. All of the trajectories show similar characteristics in which there is a sharp rise in the distance of the iron from the heme plane over a period of approximately 50 fs, and the iron continues to oscillate during the period plotted (0.5 ps) without any further

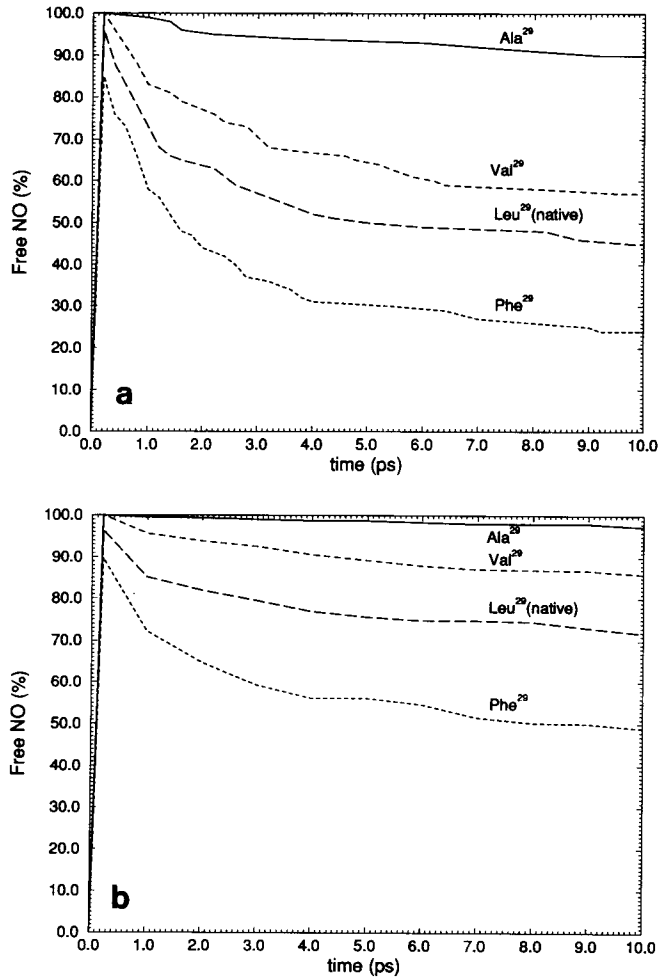

FIG. 3. **Geminate recombination curves for nitric oxide to myoglobin mutants at the 29 position.** An attempt is made to mimic experimental curves in which the concentration of the free heme (or free nitric oxide) is measured. The concentration of the free NO as a function of time is calculated directly from the semiclassical trajectories and is plotted as a continuous curve: (*a*) $\Delta = 200$ cm^{-1}; (*b*) $\Delta = 100$ cm^{-1}. *Curve b* agrees better with the experimental data.

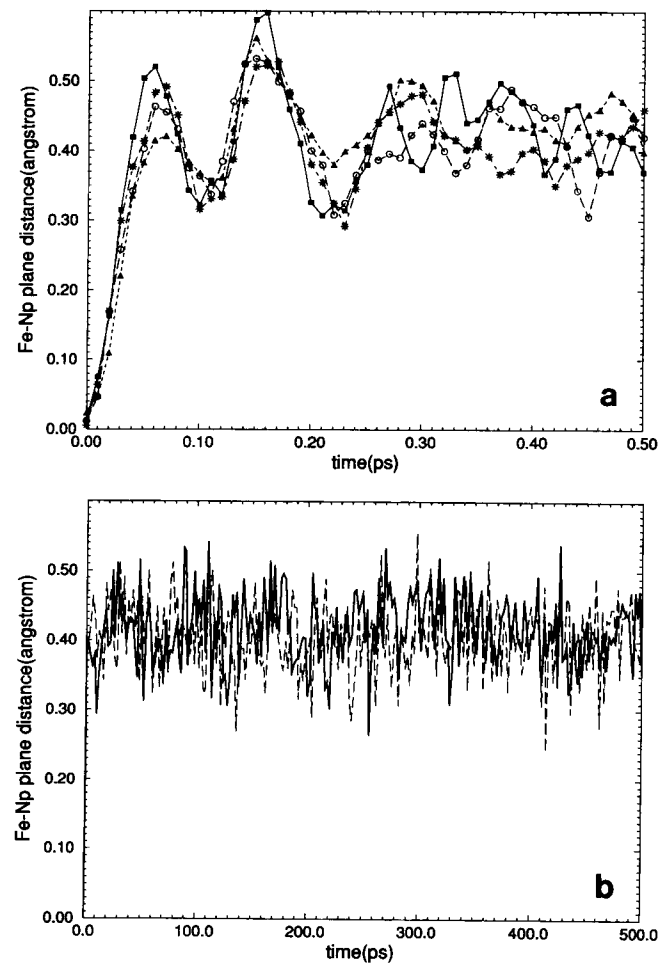

FIG. 4. **The relaxation of the dissociated heme iron from the in-plane to the out-of-plane position in myoglobin mutants.** *Np* is the pyrrole nitrogen and the distance calculated is from the iron to the average coordinate of the four pyrrole nitrogens. The distance is shown as a function of time: *a*, the short time relaxation (up to 0.5 ps) of the iron in four different trajectories of Phe^{29}. *b*, longer time behavior of the relaxation. Two trajectories of 500 ps of alanine 29 (*dashed line*) and of phenylalanine 29 (*solid line*) are shown.

apparent relaxation. In Fig. 4*b* we show the long time behavior of the iron relaxation; no longer relaxation time beyond a few picoseconds is observed. Similar results for the heme relaxation were obtained by an independent and parallel study of NO recombination by Eaton *et al.* (28).[2] The properties of the heme relaxation are not sensitive to the mutant that we consider (see Fig. 4*b* for the iron relaxation in the Ala^{29} and Phe^{29} mutants). This is not unexpected, since the 29 residue is not touching the heme directly. These results are in disagreement with the earlier simulation of Petrich *et al.* (26) that identified long time relaxation. The similarities of the heme relaxation times in all the mutants suggest that other properties of the heme are the same as well. Within the limits of our mechanical model, we were not able to identify any changes in heme properties in the myoglobin mutants. However, *large variations in recombination rates* for different mutants are observed in the theory and the experiment (see Fig. 3 and Ref. 11). This argues against a dominant role of heme relaxation processes in the geminate recombination. It was suggested (26), based on indirect evidence, that heme relaxation is the reason for the non exponential kinetics of the recombination. That is, a time-dependent barrier for NO recombination is induced by the iron displacement out of the plane, and this barrier is responsible for the 100-ps recombination kinetics. According to the present simulation, previous approximate simulations (11), and the recent experiment (29) it is unlikely that a significant barrier for NO recombination is present at the heme. Analysis of the present simulations suggests that NO geminate recombination is controlled by diffusion in the heme pocket (see below). This is especially suggestive in the simulation of the Phe^{29} mutant. In this mutant the diffusion is restricted by the bulky side chain as compared to the native protein, reducing significantly the effective diffusion at short times. In the calculations the heme in the Phe^{29} relaxes (similarly to the native) to an out-of-plane position at times shorter than 1 ps. Furthermore, the ligand loses its excess kinetic energy in approximately 1 ps. For ligands that rebind at times longer than 1 ps, one expects a full heme barrier (or very close to that if a small fraction of heme relaxation is still going on (26)). Nevertheless, the observed recombination time in the experiment (11) and in the simulations is very fast. It is within the laser pulse width (35 ps) and of order of 10 ps in the simulation, suggesting negligible heme barrier for NO recombination.

[2] O. Schaad, H.-X. Zhou, A. Szabo and W. A Eaton, manuscript submitted.

Furthermore, recombination experiments in which the iron was replaced by a cobalt atom yielded kinetic behavior similar to the iron myoglobins (29). Since the cobalt heme is not displaced from the plane after dissociation, the similarity between the geminate recombination for cobalt and for iron suggests that the iron out-of-plane movement has little effect on the recombination. It is therefore impossible to explain the kinetic differences of ligand recombination in the 29 mutants in terms of heme properties only.

In Fig. 5 we show the approximate positions of the dissociated and bound ligands in the different mutants. The intermediate position of the ligand is essentially the same as the one suggested in Ref. 11 that employs the approximate LES methodology. It is at the back of the heme pocket, and the nearby residues are shown in Fig. 1. To appreciate the difference in the extent of ligand motion for the different mutants, we show in Fig. 6 a histogram plot of the number of collisions of the ligand with the pocket residues. A collision is defined by an encounter of less than 4 Å between any of the ligand atoms and any of the residue atoms. Each *box* in the figure represents the result of a single trajectory. The *boxes* are arranged so that the largest number of collisions is on the right and the smallest number is on the left. It is evident that there is a large variability in collision numbers even for the same mutant, indicating that the protein is not self-averaging during a single trajectory of the ensemble of trajectories calculated for that 29-mutant. Our sample of trajectories could be improved in size, especially considering the large variations in collision numbers. Also, the initial conditions could be prepared more independently from a high temperature trajectory (12, 27). Nevertheless, the ordering of the collision numbers for the different mutants is $Phe^{29} > Leu^{29} > Val^{29} >$ Ala29 in accord with the experimental recombination rate (larger collision number reflects smaller volume explored). Hence, estimates that inversely correlate the accessible volume to ligand diffusion with the recombination rate (11) are consistent with the results of the present calculations in which the rate is computed directly.

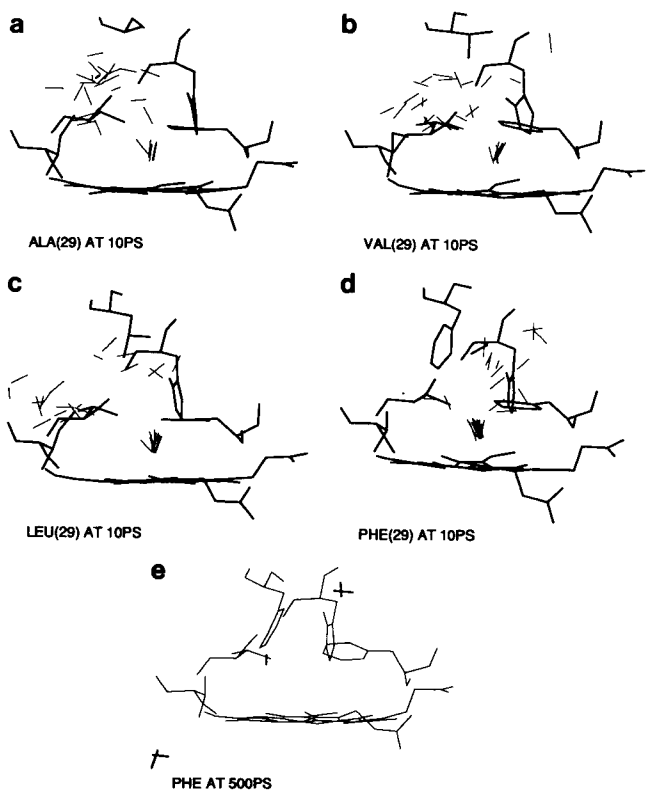

FIG. 5. **The final positions of the ligands at the end of the 10-ps trajectories for the different mutants.** For clarity only a single protein structure is shown. The protein was (of course) fluctuating during the simulation. In addition to the heme, the plot includes the residues: *a*, Ala; *b*, Val; *c*, Leu; *d*, Phe^{29} also shown, Phe^{43}, His^{64}, Val^{68}, and Ile^{107}. Note that the distribution of the ligands that *did not rebind* is not very different for the alternate mutants and the few ligands that succeeded to escape in phenylalanine 29 are quite far (on the average) from the heme pocket. *e* shows the position of ligands that did not rebind after 500 ps simulation of Phe^{29}.

Another question is related to differences in protein dynamics in the series of the mutants. In Fig. 7 we show the backbone fluctuations of a typical trajectory for each of the mutants measured with respect to the starting structure as a function of time. All trajectories show comparable curves with maximum fluctuations of 1 Å. Fluctuations averaged over the whole trajectory as a function of the residue number are shown in Fig. 8 and are quite similar for the different proteins. Hence, the mutations do not affect the global fluctuations of the proteins compared to the wild type, and the effects of the structural changes are confined to the close neighborhood of the heme pocket.

The following puzzle in the long time behavior deserves consideration. In Ref. 11 it was pointed out that on the nanosecond time scale the recombination of the mutant Phe^{29} is *slower* than that of Ala^{29}. This is an opposite trend to what is found on the short time scale. To explore the reason for this opposite effect, it is necessary to extend the time scale. The long time behavior for the two mutants Ala^{29} and Phe^{29} was examined. For each of the proteins, trajectories that did not rebind after 10 ps were picked, and new trajectories of length 500 ps were computed to examine the long time recombination kinetics. 18 trajectories were calculated for the Phe^{29} mutant and another 18 trajectories were computed for the Ala^{29} mutant. Seven of the Phe trajectories and 13 of the Ala trajectories rebind. Furthermore, most of the Phe trajectories that rebind do so in the first 10 ps of the simulation and therefore can still be considered as a part of the fast phase. In contrast, the alanine recombination events are spread through the entire time period. Hence the actual "speed up" of alanine *versus* phenylalanine recombination may be even larger than suggested by the above numbers. Although the statistics are quite poor, considering the very different behavior in the short time limit, the results appear consistent with experiment. According to our model the experimentally observed opposite trend in short and long time behavior is explained as follows. The phenylalanine residue blocks the re-entrance of the ligand to the heme pocket from the interior of the protein. In the Phe simulation, two "waiting" sites for the ligand at the long time scale were identified. One of them is in the EF/heme corner, and the second is close to the CD loop (Fig. 5*e*). The re-entrance to the heme pocket from the waiting sites requires passing again the bulky phenylalanine ring. This should be contrasted with the smaller barrier that the alanine residue presents for ligand diffusion. Moreover, the phenylalanine blocks the cavity at the B/G contact (up and to the left in Fig. 5) forcing the ligand to migrate to an alternate waiting site at the E/F contact. The last cavity is accessible only by crossing a significant barrier. In contrast to the phenylalanine mutant, it was not possible to identify a structurally well defined waiting site for the alanine. The small alanine residue enables free movement from the B/G cavity to the heme pocket and *reduces* the spatial constraints on the ligand as compared to the native protein. Hence, the alanine mutation results in essentially free ligand diffusion between the B/G cavity and the heme pocket while the

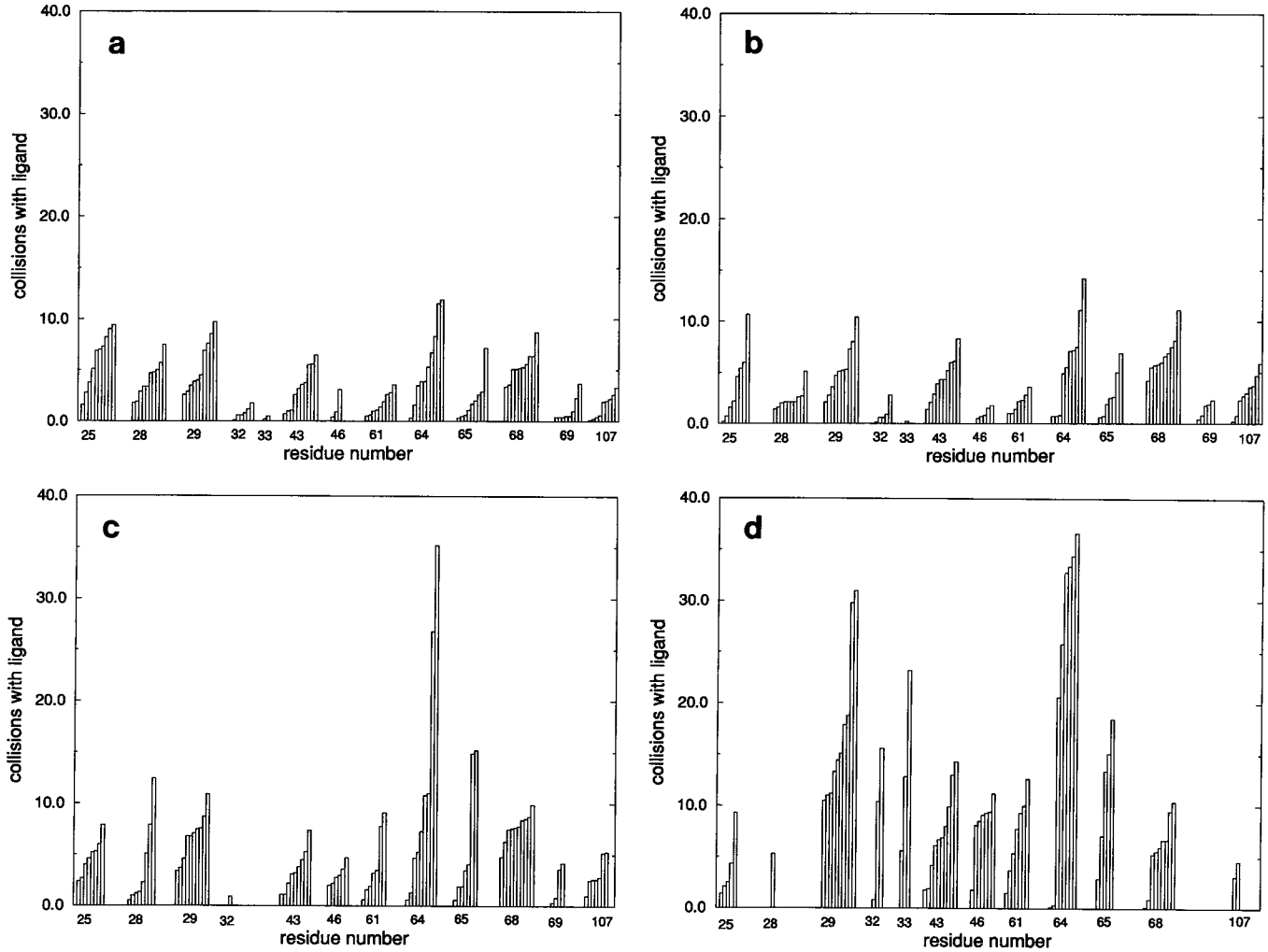

FIG. 6. **The average number of ligand collisions/picosecond with a number of critical residues close to the heme pocket.** A collision is defined to occur if at least one of the atoms of the ligand and one of the atoms of the residue are within a distance of 4 Å. For each residue there are 10 *boxes*. The *height* of a *box* represents the number of collisions in a single trajectory. The *boxes* are arranged in ascending order of collision numbers: *a*, alanine 29; *b*, valine 29; *c*, leucine 29 (wild type); *d*, phenylalanine 29.

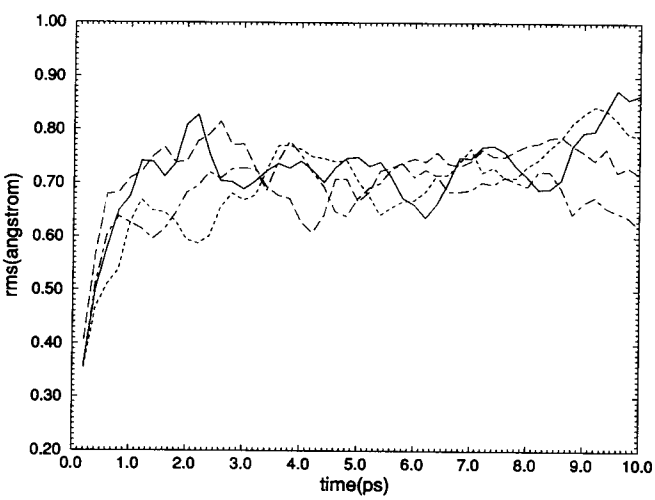

FIG. 7. **The backbone root-mean-square for 10 ps trajectories of the myoglobin mutants: *solid line*, alanine 29; *long dashed line*, valine 29; *dot dashed line*, leucine 29 (wild type); *short dashed line*, phenylalanine 29.** Note the small differences between the four trajectories.

phenylalanine mutation results in activated diffusion.

In the experiment (11) a slow phase for alanine (a single diffusion process) is observed. In the phenylalanine a biphasic behavior (well separated, fast and slow processes) were extracted from the experimental data. The above observations are consistent with free diffusion for the alanine and activated diffusion for the phenylalanine as suggested by the simulations. The idea of a barrier for re-entrance to the heme pocket of the phenylalanine 29 mutant was suggested in Ref. 11, based on the kinetic data only. Structural and dynamic interpretations supporting this suggestion are provided here.

DISCUSSION AND CONCLUSIONS

This paper provides a complete mechanical model for the calculation of the geminate recombination of NO to myoglobin and myoglobin mutants. Based on kinetic data for four different myoglobin mutants and additional thermodynamic and spectroscopic data, we constructed a mechanical model that is in semiquantitative agreement with the available experimental data. Both short time scales (picoseconds) and long time scales (hundreds of picoseconds) were examined. The calibration of the model was made using short time data; however, using this model we were able to account also for the long time behavior. The experimental results were inter-

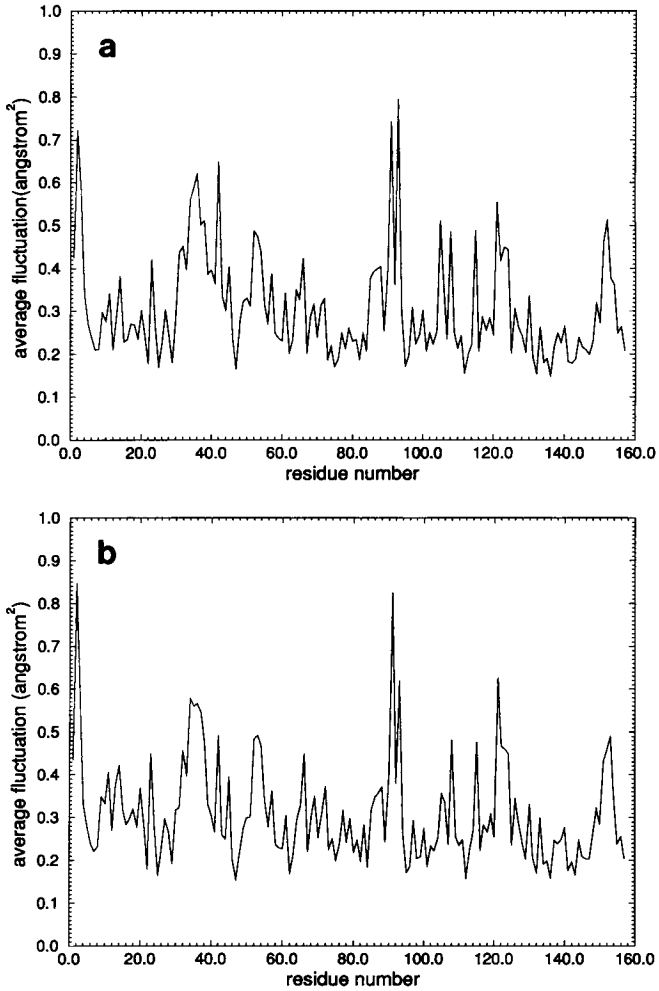

FIG. 8. **The fluctuations of individual residues with respect to the average structure of the two mutants leucine 29 (wild type) (*a*) and alanine 29 (*b*).** The average is over a 10-ps trajectory.

preted in terms of activated and free diffusion of the ligand (nitric oxide) in the protein matrix.

This is not to say that the potential and the mechanical models proposed are unique. The data on the excited state are limited. It is quite likely that the excited state can be represented in more than one way and still give results consistent with the experimental data. In the present study we adopted Ockham's razor and developed the simplest possible model that in our view contains the important features of the process and at the same time reproduces at least qualitatively the data available to us. However, we are unable to distinguish (for example) between a larger barrier along the ligand-iron coordinate and smaller electronic coupling.

We comment that we examined a model simpler than the one employed in this paper and found that it does not work. In the simpler approach the recombination was modeled by the motion of the nuclei on a *single* energy surface, *i.e.* the picture was adopted in which the system relaxes very fast to the ground state and continues its motion on a single electronic surface. The results of trajectory simulations using the above picture were very clear: all the ligand trajectories recombine on very short times, irrespective of the initial translational energy of the ligand. Thus, it seems necessary to include a minimum of two curves in order to form a bottleneck along the iron-ligand coordinate and to slow down the recombination. The conclusion that it is necessary to have a barrier in order to get the correct time scale for recombination was reached independently by another group of Schaad *et al.*[2] who simulated NO recombination to myoglobin mutants. In their model the ligand moves on a single energy surface, and no barrier is present for the reapproach of the ligand to the heme iron. The calculated recombination rate was considerably faster than experiment.

We comment that the data on the four different mutants are very valuable in constraining the model for the shape of the electronic excited state. While attempting to reproduce all the qualitative experimental observations we obtained a fairly good idea of where the crossing point should be located and what the size of coupling is between the two curves.

For example, the Phe^{29} mutant for which the recombination is the fastest suggests an upper bound for the position of the crossing point. A crossing point that is too close to the 29-residue *slows down* the recombination in the Phe^{29} mutant. The ligand collides with the phenylalanine ring that blocks its way to the crossing point. Therefore, the system cannot switch between the repulsive and the bonding curves, and ligand recombination is prevented. That sets an upper bound on the distance of the crossing point from the iron. On the other hand the crossing point cannot be set too close. If it is too close, the ligand does not feel the nearby 29-residue and the recombination rates for all the mutants are quite similar. We therefore believe that the present position of the crossing point is quite accurate.

We are less certain about the precise shape of the repulsive curve. A "reasonable" value for the exponential decay with distance was picked and the pre-exponential term was set to be consistent with the photon energy, *i.e.* we placed the excited state so that a vertical spacing from the ground state is equal to the photon energy. This is obviously an approximation since the photon energy is only an upper bound to this difference. Empirically, we found, however, that the ligand molecules lose their excess translational energy very fast after dissociation, and the precise shape of the energy surface at the steep part of the excited state has little influence on the results. Thus, the data that we have are insufficient to determine the shape of the excited state accurately.

Another quantity for which exact information is not available (to the best of our knowledge) is the coupling constant between the two electronic curves (Δ). The variation of the recombination curves with Δ is shown in Fig. 3*b*. The value of $\Delta = 100$ cm^{-1} is the closest to the experiment.

There are several conclusions worth noting from this simulation study of NO recombination.

(*a*) It is possible to construct a simple model of two electronic curves for the interaction of NO with the heme from which we can calculate directly "raw" recombination data. The model is consistent with the experimental data currently available to us. Nevertheless, there is still a considerable degree of ambiguity in the excited state properties which we cannot resolve at present.

(*b*) The present investigation supports the conclusions of previous (approximate, LES) simulations of ligand diffusion (11), *i.e.* that the rate of recombination is determined by transient and permanent cavities in the protein matrix and that the first "waiting" site of the ligand is in the back of the heme pocket.

(*c*) The simulations are in disagreement with the model of heme relaxation (26). In this model a time-dependent barrier to the ligand recombination is associated with the displacement of the iron out-of-plane. Within our model, which uses a different potential energy function for the protein, the heme relaxation is much faster than the recombination process considered (approximately 1 ps).

The heme relaxation was very similar in all mutants. The differences in the recombination rate of the four mutants are accounted for entirely by the free volume accessible for ligand diffusion.

(*d*) Using the new model, it is also possible to explain the difference between the short time and the long time behavior of Ala^{29} and of Phe^{29}. Thus, at short times the Phe^{29} squeezes the ligand against the heme, and the recombination is fast. However, at long times the ligand is no longer in the original binding cavity. The large phenylalanine ring prevents the diffusion of the ligand to the nearest cavity at the B/G contact and forces the ligand to a different cavity at the E/F corner or to the CD loop. From the last two positions, the re-entrance to the binding site is associated with a barrier. Thus, once the ligand passed the phenylalanine ring it is much harder for it to re-enter the binding site. The alanine does not prevent diffusion to the B/G cavity; on the contrary, its smaller size compared to the native protein residue (leucine) reduces the already small barrier even further. At short times the ligand in the alanine mutant easily escapes from the binding site but it also easily returns to it at longer times. Therefore, the long time recombination shows an opposite trend to the short time.

Acknowledgments—We thank Prof. Q. H. Gibson for many delightful discussions and for pointing out the need for a complete model of the recombination process and Prof. E. Gislason for helpful discussions and for directions to important references.

REFERENCES

1. Elber, R., and Karplus, M. (1990) *J. Am. Chem. Soc.* **112,** 9161–9175
2. Kottalam, J., and Case, D. A. (1988) *J. Am. Chem. Soc.* **110,** 7690–7697
3. Nowak, W., Czerminski, R., and Elber, R. (1991) *J. Am. Chem. Soc.* **113,** 5627–5637
4. Verkhivker, G., Elber, R., and Gibson, Q. H. (1992) *J. Am. Chem. Soc.* **114,** 7866–7878
5. Olson, J. S., Mathews, A. J., Rohlfs, R. J., Springer, B. A., Egeberg, K. D., Sligar, S. G., Tame, J., Renaud, J. P., and Nagai, K. (1988) *Nature* **336,** 265–266
6. Smerdon, S. J., Dodson, G. G., Wilkinson, A. J., Gibson, Q. H., Blackmore, R. S., Carver, T. E., and Olson, J. S. (1991) *Biochemistry* **30,** 6252–6260
7. Lambright, D. G., Balasubramian, S., and Boxer, S. G. (1991) *J. Mol. Biol.* **207,** 289–299
8. Carver, T. E., Brantley, R. E., Jr., Singleton, E. W., Arduini, R. M., Quillin, M. L., and Phillips, G. N., Jr. (1992) *J. Biol. Chem.* **267,** 22022–22034
9. Adachi, S., Sunohara, N., Ishimori, K., and Morishima, I. (1992) *J. Biol. Chem.* **267,** 12614–12621
10. Austin, R. H., Beeson, K. W., Eisenstein, L., Frauenfelder, H., and Gunsales, I. C. (1975) *Biochemistry* **14,** 5355–5373
11. Gibson, Q. H., Regan, R., Elber, R., Olson, J. S., and Carver, T. E. (1992) *J. Biol. Chem.* **267,** 22022–22034
12. Straub, J. E., and Thirumalai, D. (1993) *Proteins* **15,** 360–373
13. Weiner, S. J., Kollman, P. A., Case, D. A., Singh, U. C., Ghio, C., Alagons, G., Profeta, S., Jr., and Weiner, P. (1984) *J. Am. Chem. Soc.* **106,** 765–784
14. Jorgensen, W. L., and Tirado-Rives, J. (1988) *J. Am. Chem. Soc.* **110,** 1657–1666
15. Brooks, B. R., Bruccoleri, R. E., Olafson, B. D., States, D. J., Swaminathan, S., and Karplus, M. (1983) *J. Comp. Chem.* **4,** 187–217
16. Kuczera, K., Kuriyan, J., and Karplus, M. (1990) *J. Mol. Biol.* **213,** 351–373
17. Waleh, A., and Loew, G. H. (1982) *J. Am. Chem. Soc.* **104,** 2346–2351
18. Gibson, Q. H. (1957) *Proc. R. Soc. Lond. Ser. B Biol. Sci.* **147,** 44–56
19. Maxwell, J. C., and Caughey, W. S. (1976) *Biochemistry* **15,** 388–396
20. Agmon, N., and Hopfield, J. J. (1983) *J. Chem. Phys.* **79,** 2042–2053
21. Landau, L. *Z. Phys. Sov.* (1932) **2,** 46–51
22. Zener, C. (1932) *Proc. R. Soc. Edinb. Sect. A (Math. Phys. Sci.)* **137,** 696–702
23. Cline, R. E., Jr., and Wolynes, P. G. (1987) *J. Chem. Phys.* **86,** 3836–3844
24. Straub, J. E., and Berne, B. J. (1987) *J. Chem. Phys.* **87,** 6111–6116
25. Frauenfelder, H., and Wolynes, P. G. (1985) *Science* **229,** 337–345
26. Petrich, J. W., Lambry, J. C., Kuczera, K., Karplus, M., Poyart, C., and Martin, J. L. (1991) *Biochemistry* **30,** 3975–3989
27. Straub, J. E., and Thirumalai, D. (1993) *Proc. Natl. Acad. Sci. U. S. A.* **90,** 809–813
28. Henry, R., Levitt, M., and Eaton, W. A. (1985) *Proc. Natl. Acad. Sci. U. S. A.* **82,** 2034–2038
29. Ikeda-Saito, M., Dou, Y., Yonetani, T., Olson, J. S., Li, T., Regan, R., and Gibson, Q. H. (1993) *J. Biol. Chem,* **268,** 6855–6857